1998

Dynamics Prediction of Refrigerant Rotary Compressor Crankshaft

R. Dufour
INSA de Lyon

M. Charreyron
Tecumseh Europe

M. Gerard
Tecumseh Europe

DYNAMICS PREDICTION OF REFRIGERANT ROTARY COMPRESSOR CRANKSHAFT

Régis Dufour
INSA de Lyon, Laboratoire de Mécanique des Structures, UPRESA CNRS 5006, 69621 Villeurbanne, France

Michel Charreyron and **Maryline Gérard**
Tecumseh Europe, Service Etude, 38290 La Verpillière, France

Abstract

This paper concerns the prediction which must be performed at the design stage in order to implement a mechanical solution to avoid an over-pronounced lateral deflection of the rotor-crankshaft assembly of a refrigerant rotary compressor capable of variable speeds of rotation. Experimental modal analyses carried out on several items of rotor-crankshaft assemblies permit establishing a reliable Finite Element model used for predicting the effect on the unbalance response of the clearance of the fluid film bearings, which have speed of rotation dependant parameters. It is shown that an increase of the radial bearing clearance solves the mechanical problem partially.

1- INTRODUCTION

In the refrigerant rotary compressor under study, see Figs. 1 and 2, the rolling piston is capable of running from 1,200 to 7,200 rpm. Schematically the electric stator is fixed to a crankcase which is welded by three spots to the hermetic housing vertically mounted on three grommets. Contrary to the reciprocating compressors, there is no internal suspension [1]. The crankshaft fitted into the overhung electric rotor, is mounted on two fluid film bearings: the main and the outboard bearings.

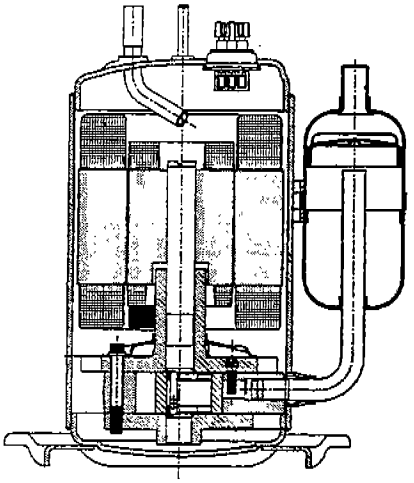

Figure 1. Rotary compressor

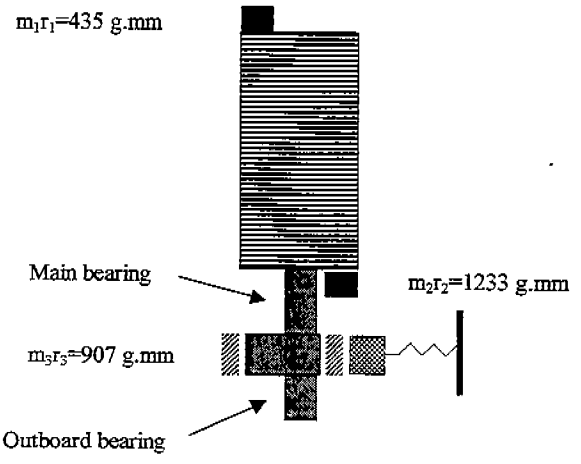

Figure 2. Mass unbalance

The crankshaft drives the crank mechanism comprising mechanical parts (the eccentric, the piston rolling in a cylinder, and the vane-spring system) which have eccentric masses. The counterweight masses (m_1r_1 and m_2r_2, see Fig. 2), located at the top and the bottom of the rotor are designed to reduce the effect of the mass unbalance (m_3r_3). Thus there is an mass unbalance combination which induces mechanical damage at the highest speeds of rotation, in particular rotor-to-stator rubs and failures at the crankcase weld spots. Therefore it is necessary, at the design stage, to use a model for predicting the lateral response, especially the unbalance response of the rotor-crankshaft assembly, to better understand the dynamic behavior and to implement suitable and realistic modifications. This paper deals with such a theoretical prediction which is experimentally validated by modal analysis at rest. Firstly, experimental modal analysis carried out on rotor-crankshaft assemblies permits updating of the corresponding finite element modeling at rest. Secondly, the damping and stiffness coefficients of the bearings, which are speed of rotation dependant are taken into account for predicting the steady state unbalance response. These calculations are performed

for three sets of bearing clearances. In this paper, which completes [2], the prediction uses the theory and SYSROTOR computer program described in [3].

2- NATURAL FREQUENCIES OF THE ROTOR-CRANKSHAFT ASSEMBLY WITHOUT BEARINGS

This step consists in establishing a reliable model of the rotor-crankshaft assembly in bending. The crankshaft is made of cast-iron. The steel laminations joined together with aluminum bars compose the electric rotor. They make the rotor flexible. Therefore the lateral stiffness of the electric rotor and the clamping point of the crankshaft fitted into the rotor are insufficiently controlled.

Experimental Modal Analyses

The experimental modal analyses are carried out on a crankshaft alone and then on a set of rotor-crankshaft assemblies, see Figure 3, to obtain average values of the natural frequencies of items with free-free boundary conditions. The natural frequencies and mode shapes are measured in the two bending planes using the classical sine wave and/or impact analyses.

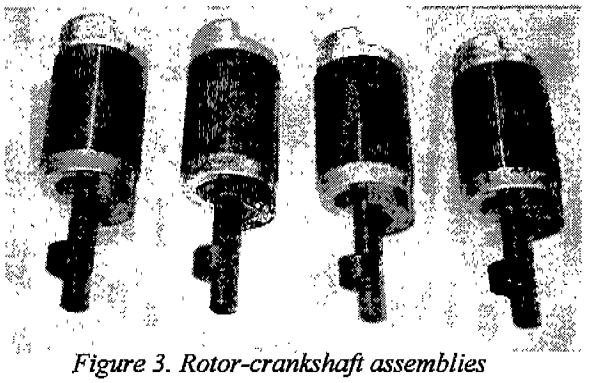

Figure 3. Rotor-crankshaft assemblies

Finite Element Model

The Y axis is along the rotation axis of the crankshaft, the origin being the abscissa of the counterweight mass located at the top of the rotor. XY and ZY are the bending planes. Let each node contain four degrees of freedom: two translations and two slopes. The beam elements have two nodes while the mass elements have only one node. Figure 4 presents schematically the FE model of the rotor-crankshaft assembly which corresponds to the experimental modal analysis tests carried out to update the model. The italic labels are dedicated to the element number while the others concern the nodes.

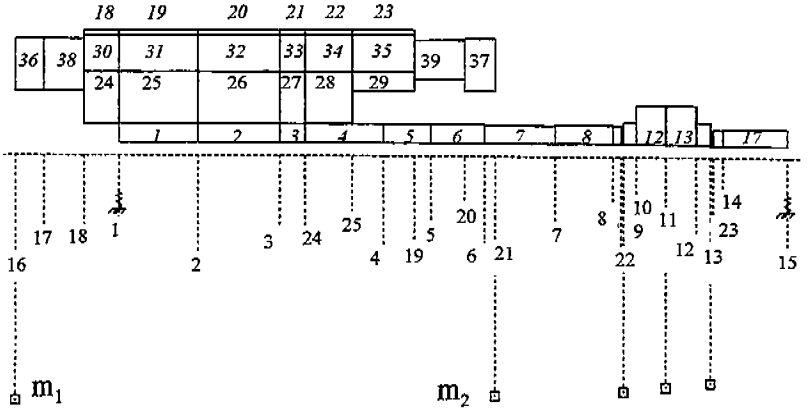

Figure 4. Finite element model of the rotor-crankshaft assembly

Beam element number	Mechanical parts	Young modulus (N/m^2)	Mass density (kg/m^3)
1 to 17	Crankshaft	$1.75\ 10^{11}$	7300
18 to 29	Steel laminations without aluminum	$0.05\ 10^{11}$ (from experimentation)	7800
30 to 35	Steel laminations (50%) and aluminum bars (50%)	$(0.7\ 10^{11} + 0.05\ 10^{11})/2$	(7800 + 2700)/2
38 and 39	Aluminum ring	$0.7\ 10^{11}$	2700
36 and 37	Link of counterweight masses (nodes 16 and 21)	$15.0\ 10^{11}$	1

Table 1. Material characteristics of the beam elements

Table 1 summarizes the material characteristics of the beam elements. The counterweight masses (m_1 and m_2), eccentric masses (eccentric, shoulders), and eventually the accelerometer mass are modeled using mass elements. Bearing elements having slight stiffness (located at nodes 1 and 15) are introduced in order to take into account the rubber band of the experimental boundary conditions. The calculation of the kinetic energy, strain energy, virtual work and the application of Lagrange's equations yield the following set of equations:

$$[M]\{\ddot{X}\}+[K]\{X\}=0 \qquad (1)$$

with *{X}* being the displacement vector containing the DOF of the structures, *[M]* the mass matrix and *[K]* the stiffness matrix. The natural frequencies and the mode shapes are sought by solving Equations (1).

Numerical and Experimental Results

The crankshaft model is validated by the experimentation, (the results are not presented). The experimentation on the four rotor-crankshaft assemblies permits updating the lateral stiffness of the electric rotor and the location of the clamping point of the crankshaft. Note that the adjacent beam elements 28 and 4 are connected to node 24. Table 2 presents the first two natural frequencies in the ZY bending plane, a 17 gram accelerometer being placed at the abscissa of the node 18. The FE model of the rotor-crankshaft assembly at rest is satisfactory.

	Assembly	f_1 (Hz)	f_2 (Hz)
Experimentation	*1*	961	4984
	2	969	5032
	3	968	5024
	4	984	5108
	Average	**970**	**5037**
Computation	***F.E. model***	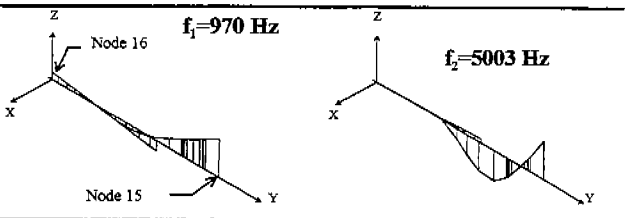	

Table 2. Natural frequencies of the rotor-crankshaft assembly in bending

3- MASS UNBALANCE RESPONSE

The crankshaft assembly is mounted on two fluid film bearings and subjected to harmonic forces due to the unbalance masses and to the pressure acting on the rolling piston and thus on the eccentric. Above 1,000 rpm the mass unbalance forces have a predominant effect on the bending motion of the assembly [2]. So the following investigation focuses only on the mass unbalance response with special attention being given to the bearing clearance.

	Main bearing		Outboard bearing
	Bearing #1	Bearing #2	Bearing #3
Length / Diameter	26/16	14/16	15/14.3
F (N)	144	144	512
Clearance A (μm)	6.5	6.5	5
Clearance B (μm)	9	9	7.5
Clearance C (μm)	14	14	12.5

Table 3. Bearing characteristics

Modeling of the Rotor-Crankshaft Assembly on Bearings

Let the assembly be symmetric in order to avoid solving a system with periodic coefficients. Let the main bearing be split into two bearings (bearings #1 and #2) due to a middle groove and the outboard bearing be referred to as bearing #3. Let the hermetic housing have no motion. Therefore the unbalance response of the assembly mounted on three bearings is predicted solving the following equations:

$$[M]\{\ddot{X}\}+[C(\Omega)+C_I(\Omega)]\{\dot{X}\}+([K]+[K_I(\Omega)])\{X\}=\{F(\Omega)\} \qquad (2)$$

where, displacement vector *{X}* contains all the DOF of the FE model, *[M]* and *[K]* are the classical mass and stiffness matrices, *[C(Ω)]* is the non symmetric gyroscopic matrix which depends on the speed of rotation Ω, *[C_I(Ω)]* and *[K_I(Ω)]* are the damping and stiffness matrices of the bearings; *{F(Ω)}* being the harmonic force vector. The harmonic force vector *{F(Ω)}* includes the two forces due to each unbalance mass: m_1, m_2 and a mass which involves the masses of the eccentric, shoulders, rolling piston, and vane.

$$f_X = mr\Omega^2 \cos(\Omega t+\Phi) \qquad f_Z = mr\Omega^2 \sin(\Omega t+\Phi) \qquad (3)$$

The bearings are modelled with one-node elements having two lateral translations. The springs of the FE model, (Fig. 4), are removed. Bearing#1 is located at node 5 while bearings #2 and #3 are situated at the middle of elements 8 and 17, respectively. Their stiffness K_{ij} and damping C_{ij} characteristics are speed of rotation dependant and are calculated according to the relationships:

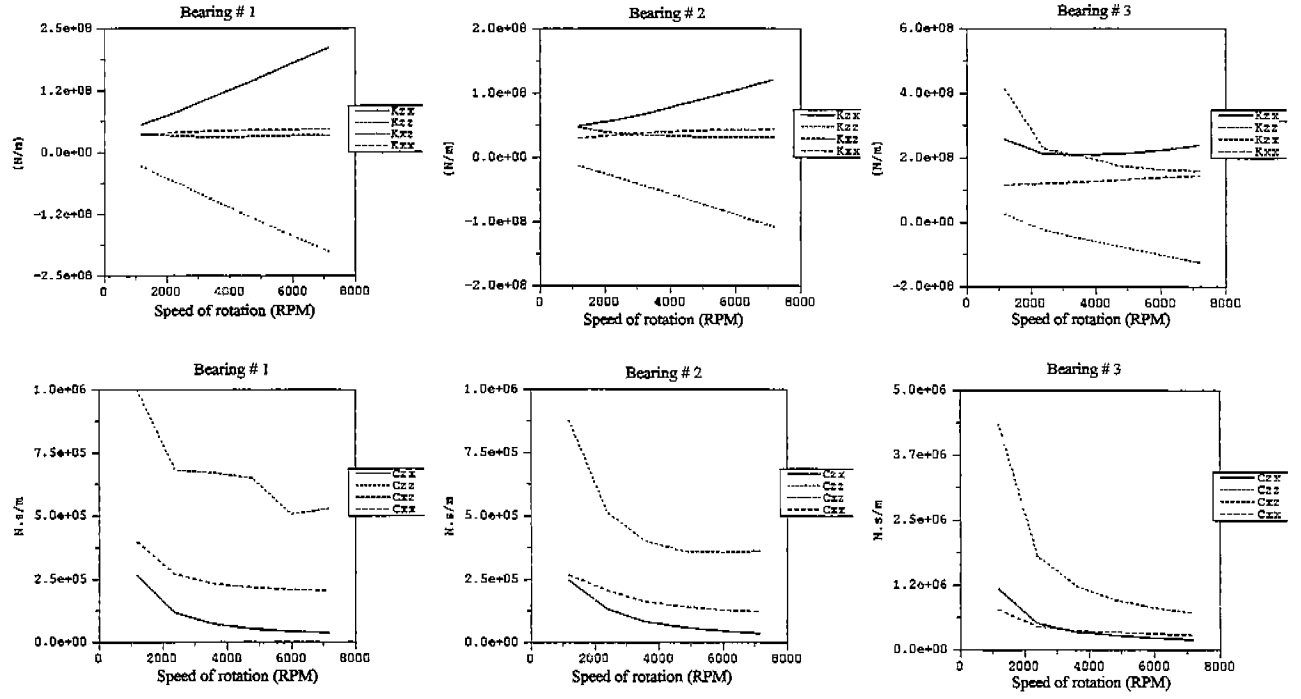

Figure 5. Stiffness and damping coefficients of bearings versus speed of rotation, (bearing clearance B)

$$K_{ij} = k_{ij}(S)\frac{F}{C_p} \qquad C_{ij} = c_{ij}(S)\frac{F}{C_p\Omega} \tag{4}$$

where C_p is the bearing clearance, F the static load [4], and k_{ij} and c_{ij} non-dimensional coefficients given in [5] and depend on the Sommerfeld number S. Three types of bearing clearance are taken into account: A, B and C. Table 3 shows the bearing characteristics while Figures 5 presents, for example, the stiffness and damping coefficients of the three bearings in the 1,200-7,200 rpm range and for the mean clearance B. The solution of the system

$$[M]\{\ddot{X}\}+([K]+[K_J(\Omega=0)])\{X\}=0 \tag{5}$$

gives the modal basis. Then the pseudo-modal method is used to reduce the number of the Eqs. (2). The harmonic solution is sought for different speeds of rotation.

Results

The mass unbalance response, plotted in Figure 5 concerns the top of the rotor (node 18), and the centres of the three bearings and Figure 7 shows the assembly deflection at 7,200 rpm.

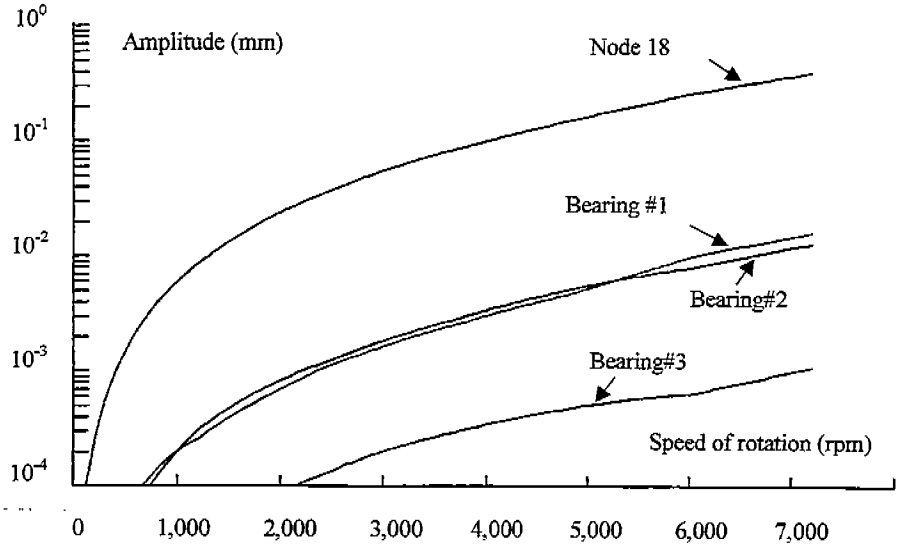

Figure 6. Mass unbalance response, bearing clearance B

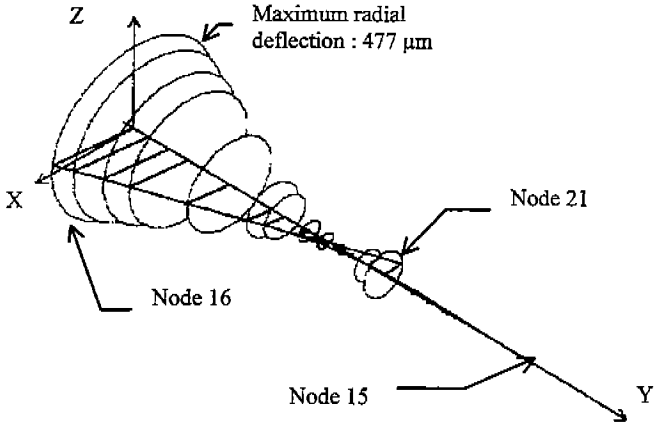

Figure 7. Mass unbalance response. Rotor-crankshaft deflection at 7,200 rpm

Bearing clearances	A	B	C
Rotor-stator gap, node 18 (mm)	0.3	0.3	0.3
Speed of rotation (rpm)	6,600	6,300	6,200
Bearings #1 node 5 (µm)	6.5	9	14
Speed of rotation (rpm)	5,250	5,800	6,000

Table 4. Predicted speed of rotation limit values

It should be noticed that there is no resonance phenomena within the 0-7,200 rpm range. The amplitude displacement increases with the speed of rotation. The predicted response with the two other sets of bearing clearance have roughly the same shape. There is a difference only regarding the amplitude, see Table 4 which gives the speeds of rotation at which the rotor-stator gap or the bearing # 1 clearance are reached. It is shown that the rotor-to-stator rub occurs from 6,200 rpm (clearance C) while the contact at the bearing #1 occurs from 5,250 rpm (clearance A). The mechanical damages (rotor-to-stator and bearing rubs) have been observed experimentally during prototype tests. Bearing #1 is subjected to the highest efforts contrary to bearing #3 (the outboard bearing). Table 5 summarizes the predicted efforts at bearing #3 for the three kinds of clearances and shows that the effort increase with the speed of rotation and clearance A induces the highest efforts.

Clearances	A		B		C	
Efforts (N)	**FX**	**FZ**	**FX**	**FZ**	**FX**	**FZ**
1,200 (rpm)	7.37	17.9	3.58	5.27	0.7	2.3
2,400	31.7	57.1	15.4	22.8	5.8	1.5
3,600	40.6	110	28.6	50.6	19.2	39.2
4,800	127	263	37.7	109	44.3	82.4
6,000	183	408	52.7	211	95.4	156
7,200	528	897	149	415	198	271

Table 5. Outboard bearing efforts versus speed of rotation

4. CONCLUSION

The FE model updated with modal analysis tests carried out at rest permits predicting the response of the rotor-crankshaft assembly subjected to different types of solicitations. Regarding the mass unbalance response the prediction has shown that the lateral deflection of the crankshaft in bending is over-pronounced from 6,000 rpm. The smallest bearing clearance (A) reduces the lateral deflection of electric rotor but induces considerable great bearing efforts. Consequently, modification of bearing clearance partially improves the rotor dynamics of rotary compressors capable of variable speeds of rotation. In the future, hermetic housing motion and efficient balancing at low and high speed of rotation will be studied.

ACKNOWLEDGEMENTS

The authors are indebted to Tecumseh Europe Co. for its support and permission to publish this work.

REFERENCES

1. R. Dufour, J. Der Hagopian, M. Lalanne, *Transient and steady state dynamic behaviour of single cylinder compressors: prediction and experimentation*, **J. of Sound and Vibration**, 181, 23-41, 1995
2. R. Dufour, M. Gérard, M. Charreyron, *Dynamic analysis of a crankshaft in bending with an electric motor and non-linear fluid film bearing*, **IFToMM, Fifth Intern. Conf. On Rotor dynamics,** 1998
3. M. Lalanne, G. Ferraris, **Rotordynamics prediction in engineering**, 2nd edition, John Wiley & Sons, 1997
4. K.Imaichi, M. Fukushima, S. Muramatsu, N. Ishii, *Vibration of rotary compressors*, **Proceedings Purdue Compressor Technology Conf.**, 275-282, 1982
5. Tsuneo Someya, **Journal-bearing data book**, 1991, Springer-Verlag